# FLUID: Training-Free Face De-identification via Latent Identity Substitution

# Jinhyeong Park\*, Shaheryar Muhammad\*, Seangmin Lee, Jong Taek Lee, and Soon Ki Jung†

School of Computer Science, Kyungpook National University, South Korea

#### **Abstract**

We present FLUID (Face de-identification in the Latent space via Utility-preserving Identity Displacement), a training-free framework that directly substitutes identity in the latent space of pretrained diffusion models. Inspired by substitution mechanisms in chemistry, we reinterpret identity editing as semantic displacement in the latent h-space of a pretrained unconditional diffusion model. Our framework discovers identity-editing directions through optimization guided by novel reagent losses, which supervise for attribute preservation and identity suppression. We further propose both linear and geodesic (tangent-based) editing schemes to effectively navigate the latent manifold. Experimental results on CelebA-HQ and FFHQ demonstrate that FLUID achieves a superior trade-off between identity suppression and attribute preservation, outperforming state-of-the-art de-identification methods in both qualitative and quantitative metrics.

#### Introduction

The widespread deployment of face recognition (FR) systems has raised urgent concerns about biometric privacy. Facial images are permanent, uniquely identifiable, and easily captured, making them ideal for surveillance but difficult to protect. Although legal safeguards such as the General Data Protection Regulation (European Union 2016) and India's Digital Personal Data Protection Act (Government of India 2023) have emerged, technical solutions remain limited. As a result, de-identification methods are increasingly needed to protect privacy and mitigate risks such as deepfake misuse (Westerlund 2019) before visual data are shared.

Traditional de-identification techniques (e.g., masking, pixelation, and blurring) (Babaguchi et al. 2009; Ilia et al. 2015) often degrade image quality and fail against modern FR models. Recent generative models, such as generative adversarial networks (GANs) (Goodfellow et al. 2014) and diffusion models (DMs) (Ho, Jain, and Abbeel 2020) offer promising alternatives with improved realism (Wen et al. 2022; Cai et al. 2024; Shaheryar, Lee, and Jung 2025). However, while these generative methods successfully achieve more realistic identity suppression than traditional ones, they share a critical limitation: most produce visibly altered faces immediately recognizable as de-identified. This occurs

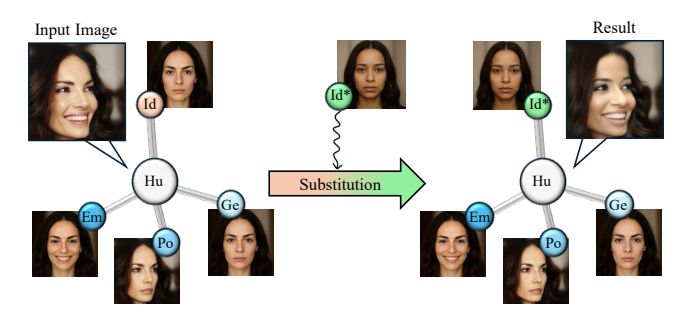


Figure 1: The concept of our approach with the metaphor of substitution reaction. Identity editing within the latent space replaces the original identity (Id) with a de-identified one (Id\*), while preserving attributes of a human face image (Hu), such as emotion (Em), gender (Ge), and Pose (Po), strictly than state-of-the-art de-identification methods.

because they often fail to preserve well-known non-identity attributes, such as emotion, pose, and gender, resulting in uncanny or artificial-looking outputs. Consequently, viewers may perceive these protected images as unnatural or suspicious, which can further undermine content authenticity and source credibility.

To address these limitations, we turn to latent-space editing, hypothesizing its superior attribute preservation compared to generative reconstruction approaches. Latent editing operates on semantically disentangled representations, allowing independent and gradual manipulation. This enables fine-grained control over the input while reflecting required changes. Recent discoveries in the latent spaces of generative models have enabled such training-free semantic image editing, where inverting input images into the latent space and editing by traversing semantic directions (e.g., emotion, color, pose) yield desired results (Härkönen et al. 2020; Shen et al. 2020; Kwon, Jeong, and Uh 2022). However, current editing methods primarily focus on attribute manipulation while preserving identity, making them unsuitable for de-identification. Moreover, prior editing often relies on inadequate prompts, model fine-tuning, or complex pre-processing pipelines (Kim, Kwon, and Ye 2022; Avrahami, Lischinski, and Fried 2022; Zhu et al. 2023; Sun et al.

To enable de-identification with strict attribute preserva-

<sup>\*</sup>These authors contributed equally.

<sup>&</sup>lt;sup>†</sup>Corresponding author.

tion, we propose FLUID (Face de-identification in the Latent space via Utility-preserving Identity Displacement), a training-free framework that performs identity substitution directly in the latent space of a pretrained unconditional DM. This space, named h-space, of unconditional DMs has been shown to provide a linear, robust, and homogeneous semantic space (Kwon, Jeong, and Uh 2022). Drawing inspiration from substitution reactions in organic chemistry (Rizzo 2005; Ashenhurst 2012a), FLUID metaphorically frames identity removal as a semantic substitution process. In this framework, we introduce a set of reagent losses, each acting as a functional analogue to chemical reagents, to control the outcome of this substitution, specifically targeting identity suppression and attribute preservation. To operationalize this concept, we explore both linear and geodesic (tangentbased) displacement strategies in latent space, enabling us to examine the trade-off between de-identification strength and attribute retention. To the best of our knowledge, we are the first to perform face de-identification in the latent space of a DM. Our contributions are as follows:

- We introduce a training-free identity substitution framework in the h-space of an unconditional DM.
- We propose a novel editing scheme inspired by substitution chemistry, optimized via differentiable reagent losses.
- We present and compare our tangent-space editing method with the common linear edit, demonstrating a strong balance between de-identification and attribute fidelity.
- We demonstrate FLUID's improved performance over training-based SOTA methods in both realism and utility preservation through extensive experiments.

#### **Related Works**

Face Image Editing. Latent space editing in generative models enables facial attribute control without retraining. Early GAN-based methods like InterfaceGAN (Shen et al. 2020) and StyleFlow (Abdal et al. 2021) identified interpretable directions for attributes (e.g., age, smile), while StyleSpace (Wu, Lischinski, and Shechtman 2021) provided fine-grained controls within StyleGAN (Karras, Laine, and Aila 2019). In DMs, latent traversal has been explored via hspace in Asyrp (Kwon, Jeong, and Uh 2022), Boundary Diffusion (Zhu et al. 2023), and semantic latent discovery (Haas et al. 2024). However, these works focus on attribute editing with identity preservation. Our work inverts this paradigm, proposing identity-shifting via optimization in the h-space of an unconditional DM preserving non-identity attributes while removing identity. Unlike previous works, we treat identity as an instance-specific component and show it can be decoupled via direction optimization. Our reagent lossguided editing balances attribute consistency and identity suppression, without retraining.

Facial De-identification. Traditional privacy methods, including blurring and masking (Babaguchi et al. 2009;

Ilia et al. 2015), compromise utility and realism. Recent approaches leverage generative models for semantic de-identification, falling into two broad categories: perturbation-based and semantic identity-shifting. Perturbation-based methods, for example, Fawkes (Shan et al. 2020), AMT-GAN (Hu et al. 2022), and DiffAM (Sun et al. 2024), introduce adversarial noise or stylized makeup to deceive FR models but maintain perceptual identity, limiting protection against human re-identification. Semantic methods like DeepPrivacy2 (Hukkelås and Lindseth 2023), Repaint (Lugmayr et al. 2022), and IDDiffuse (Shaheryar, Lee, and Jung 2024) replace facial identity altogether, improving both privacy and transferability. Face-swapping approaches such as DCFace (Kim et al. 2023) and DiffSwap (Zhao et al. 2023) require additional identity inputs, making them vulnerable to misuse in deepfake scenarios (Westerlund 2019). While most of the methods require training and additional inputs, our method requires a single input and is training-free, achieving effective de-identification.

## **Preliminaries**

**Diffusion Models.** DMs generate data through a learned denoising process, modeled as a Markov chain over T timesteps. The forward process gradually corrupts clean data  $x_0$  with Gaussian noise:

$$q(x_t|x_{t-1}) = \mathcal{N}(x_t; \sqrt{1 - \beta_t} x_{t-1}, \beta_t \mathbf{I}), \tag{1}$$

where  $\beta_t \in (0,1)$  is the variance schedule. The reverse process, parameterized by a U-Net (Ronneberger, Fischer, and Brox 2015)  $\epsilon_{\theta}$ , aims to recover clean samples from noise:

$$p_{\theta}(x_{t-1}|x_t) = \mathcal{N}(x_{t-1}; \mu_{\theta}(x_t, t), \Sigma_{\theta}(x_t, t)).$$
 (2)

The mean is computed as:

$$\mu_{\theta}(x_t, t) = \frac{1}{\sqrt{\alpha_t}} \left( x_t - \frac{\beta_t}{\sqrt{1 - \bar{\alpha}_t}} \epsilon_{\theta}(x_t, t) \right), \quad (3)$$

where  $\alpha_t = 1 - \beta_t$  and  $\bar{\alpha}_t = \prod_{i=1}^t \alpha_i$ . The noise predictor  $\epsilon_\theta$  is a time-conditioned U-Net trained to estimate the added noise. The iterative denoising process enables precise pixellevel synthesis and surpasses GANs in image quality and diversity (Dhariwal and Nichol 2021; Stypułkowski et al. 2024).

The h-Space. Asyrp (Kwon, Jeong, and Uh 2022) identified that the bottleneck layer of the U-Net in DMs captures a semantic latent space termed h-space, which exhibits linearity and disentanglement. This space enables effective image manipulation without retraining the model. Editing is performed by modifying the latent  $h_t$  at each timestep with a semantic direction  $\Delta h$ :

$$x_{t-1} = \sqrt{\alpha_{t-1}} \mathbf{P}_t(\epsilon_{\theta}(x_t|\tilde{h}_t)) + \mathbf{D}_t(\epsilon_{\theta}(x_t)) + \sigma_t z_t, \quad (4)$$

where  $\tilde{h}_t = h_t + \Delta h$ ,  $\sigma_t$  is the noise scale, and  $z_t \sim \mathcal{N}(0, \mathbf{I})$ . The transformation  $\mathbf{P}_t$  shifts the  $x_0$  prediction based on  $\tilde{h}_t$ , while  $\mathbf{D}_t$  reconstructs the path to  $x_t$ . The key challenge is discovering semantically meaningful directions  $\Delta h$  that enable targeted edits without degrading unrelated features.

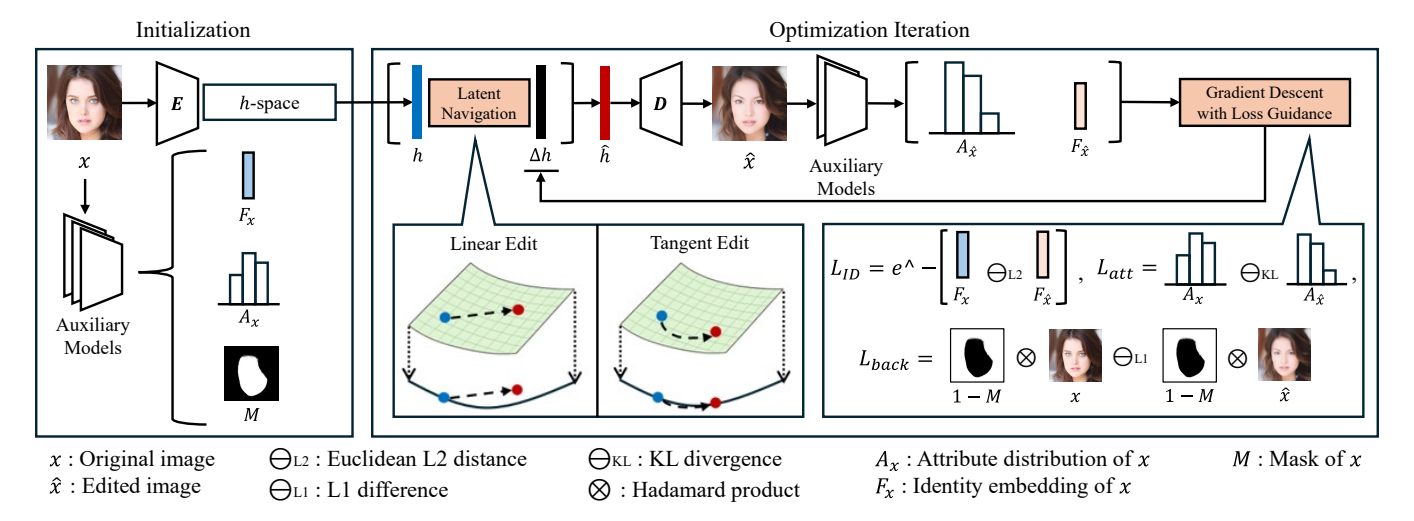


Figure 2: An illustration of our framework. In the initialization procedure, x is inverted into the latent space of a DM to obtain a starting point h, a latent vector in the h-space, while three auxiliary models are used to get  $F_x$ ,  $A_x$ , and M. During optimization, a direction vector  $\Delta h$  is iteratively guided by three loss functions to compare x and  $\hat{x}$ : an identity loss  $L_{ID}$ , an attribute preservation loss  $L_{att}$ , and a face mask loss  $L_{mask}$ . Decoding  $\hat{h}$ , the combination of h and h0, by either linear or tangent edit results in an edited image  $\hat{x}$ . Note that h1 is initialized randomly in the first optimization step.

### **Proposed Method**

This section introduces our method for training-free face de-identification using DMs through latent identity substitution. Following our chemistry-inspired framework, we remove identity information from the original image in the latent space via loss-driven optimization, then substitute a de-identified representation. Our approach operates entirely within the h-space of pretrained unconditional DMs without additional training, consisting of three key components: latent inversion, iterative optimization of identity-editing directions via differentiable losses, and reconstruction through the DM's decoder. Figure 2 provides an overview of our approach, illustrating the initialization procedure where a source image is inverted into the latent space, followed by the optimization process that uses reagent losses to guide identity substitution while preserving other facial attributes. Unlike direct latent replacement, our method discovers identity-specific directions through optimization rather than assuming prior knowledge of the identity subspace.

#### **Problem Definition**

Given a facial image  $x \in \mathbb{R}^{H \times W \times 3}$ , our goal is to generate a semantically consistent de-identified image  $\hat{x}$  such that the identity difference between x and  $\hat{x}$  is maximized, i.e.,

$$\hat{x} = \arg\max_{\tilde{x}} D_{\mathrm{id}}(x, \tilde{x}), \tag{5}$$

where  $D_{\rm id}(\cdot,\cdot)$  is an identity distance function between embeddings. Instead of directly editing in pixel space, we perform identity manipulation in the h-space of a pretrained DM. Let  $f_{\rm inv}$  be an inversion function that maps the image to its latent representation:

$$z = f_{\text{inv}}(x), \quad z \in \mathbb{R}^d.$$
 (6)

We aim to discover a direction  $\Delta h_{\mathrm{id}} \in \mathbb{R}^d$  in h-space such that applying it to z suppresses identity-related information:

$$\hat{z} = z + \lambda \cdot \Delta h_{\rm id},\tag{7}$$

where  $\lambda \in \mathbb{R}$  controls the magnitude of editing. The deidentified image is reconstructed via the DM decoder:

$$\hat{x} = \mathcal{D}(\hat{z}). \tag{8}$$

To facilitate training-free identity editing, we assume that the identity component lies in a locally linear subspace of the *h*-space. While we do not access this subspace explicitly, we optimize direction vectors guided by differentiable loss signals. Our experimental results support that these assumptions are approximately satisfied, as identity editing can be achieved without degrading other facial attributes. This builds on the empirical properties observed in recent work, such as semantic disentanglement, linear editability, and stable decoder mappings in the bottleneck features of diffusion U-Nets (Kwon, Jeong, and Uh 2022; Jeong, Kwon, and Uh 2024). We formalize the notion of latent editability and demonstrate that identity suppression and substitution can be achieved by optimizing a loss in latent space without retraining or fine-tuning the diffusion backbone.

**Definition 1.** Let  $\mathcal{D}: \mathbb{R}^d \to \mathbb{R}^{H \times W \times 3}$  denote the decoder of a pretrained DM, and let  $z = f_{\text{inv}}(x) \in \mathbb{R}^d$  be the latent representation in h-space of an input facial image  $x \in \mathbb{R}^{H \times W \times 3}$ . The identity in z is said to be *editable* if there exists a direction  $\Delta h_{\text{id}} \in \mathbb{R}^d$  such that the transformed latent code  $\hat{z} = z + \Delta h_{\text{id}}$  results in an image  $\hat{x} = \mathcal{D}(\hat{z})$  with reduced identity similarity to x while preserving all other semantics.

**Proposition 1.** Let  $z \in \mathbb{R}^d$  be the latent code of an image x, and let  $\mathcal{D}$  be a deterministic decoder corresponding to a

DM. Define the edited image as:

$$\hat{x} = \mathcal{D}(z + \Delta h_{\text{id}}),\tag{9}$$

where  $\Delta h_{id} \in \mathbb{R}^d$  is a trainable direction in latent space. Suppose the following conditions hold:

- 1. Identity attributes are embedded in a low-dimensional affine subspace  $\mathcal{H}_{id} \subset \mathbb{R}^d$ ;
- 2. The decoder  $\mathcal{D}$  is Lipschitz-continuous and differentiable with respect to its input;
- 3. The latent feature z remains approximately consistent across diffusion denoising timesteps.

Then, there exists an optimal direction  $\Delta h_{\mathrm{id}}^* \in \mathcal{H}_{\mathrm{id}}$  that minimizes a composite image-space objective:

$$\mathcal{L}_{\text{total}}(x, \hat{x}) = \alpha \mathcal{L}_{\text{id}}(x, \hat{x}) + \beta \mathcal{L}_{\text{attr}}(x, \hat{x}) + \gamma \mathcal{L}_{\text{mask}}(x, \hat{x}),$$
(10)

with  $\hat{x} = \mathcal{D}(z + \Delta h_{\mathrm{id}})$  and scalar weights  $\alpha, \beta, \gamma \in \mathbb{R}_+$ , such that identity information in  $\hat{x}$  is suppressed while other facial semantics are preserved.

Sketch of Proof. Because  $\mathcal{L}_{total}$  is differentiable with respect to  $\hat{x}$ , and  $\mathcal{D}$  is differentiable with respect to  $\Delta h_{id}$ , the composite gradient is expressed via the chain rule as:

$$\nabla_{\Delta h_{\rm id}} \mathcal{L}_{\rm total} = \nabla_{\hat{x}} \mathcal{L}_{\rm total} \cdot \nabla_{\Delta h_{\rm id}} \mathcal{D}(z + \Delta h_{\rm id}). \tag{11}$$

Condition 2 ensures that the gradients are well-behaved and bounded. Condition 1 constrains  $\Delta h_{\rm id}$  within a feasible subspace for identity transformation. Finally, condition 3 ensures that the editability holds consistently across intermediate denoising steps, as z remains stable. Therefore, training-free optimization of  $\Delta h_{\rm id}$  in latent space is both theoretically justified and practically realizable using image-level supervision alone.

#### **Latent Navigation: From Euclidean to Geodesic**

To achieve fine-grained identity editing in h-space, we implement two strategies: linear edits and tangent edits. These strategies define how the latent code  $z \in \mathbb{R}^d$  is updated during optimization using a learnable identity-editing direction  $\Delta h_{\mathrm{id}}$ .

**Linear Edit.** Linear editing is the simplest approach, where identity is modified by directly adding the editing direction to the original latent, as expressed in Equation 7. This formulation is common in latent editing literature (Kwon, Jeong, and Uh 2022; Zhu et al. 2023), and is especially effective for large semantic shifts, such as face de-identification.

**Tangent Edit.** To maintain consistency with the latent data manifold, we implement a tangent-space traversal approach, inspired by studies on geodesic editing in generative latent spaces (Hahm et al. 2024; Jeong, Kwon, and Uh 2024). Rather than applying direct linear addition, we project  $\Delta h_{\rm id}$  onto the tangent plane of the hypersphere at z. Let  $z^{\rm unit} = z/\|z\|$  and  $\Delta h_{\rm id}^{\rm unit} = \Delta h_{\rm id}/\|\Delta h_{\rm id}\|$ . The projection becomes:

$$\Delta h_{\text{proj}} = \Delta h_{\text{id}}^{\text{unit}} - \langle \Delta h_{\text{id}}^{\text{unit}}, z^{\text{unit}} \rangle \cdot z^{\text{unit}}. \tag{12}$$

Then, the geodesically traversed latent is defined as:

$$\hat{z} = ||z|| \cdot (\cos(\theta) \cdot z^{\text{unit}} + \sin(\theta) \cdot \Delta h_{\text{proj}}). \tag{13}$$

Here,  $0 \le \theta \le \pi$  is an angle given by the norm of  $h_{id}$  in radians. This way, we can still guide the latent walk's direction and intensity, consider the geodesic manifold, and eliminate a hyperparameter (i.e., editing strength  $\lambda$ ) at the same time. Linear edits offer simplicity and strong directionality, while tangent edits preserve manifold geometry for more localized and realistic transformations.

#### **Loss Functions**

To guide this latent substitution process, we introduce a set of differentiable loss functions, which we term *reagent losses*. In analogy to SN1 reactions, where different chemical reagents interact with a reactive intermediate to influence the final product, each loss function acts as a distinct supervisory "reagent" that steers the optimization toward a desired transformation. Just as protic polar solvents in SN1 stabilize intermediates and facilitate leaving group departure, our identity loss promotes effective identity removal, while attribute and face mask losses stabilize the output by preserving semantic and spatial structure. Together, these loss functions form a tunable and composable framework that enables selective identity editing in the latent space without compromising image utility.

**Identity Loss.** To ensure effective suppression of identity information, we introduce an identity loss based on FaceNet (Schroff, Kalenichenko, and Philbin 2015), a widely used FR model. The model encodes images into an embedding space where Euclidean distance correlates with identity difference. Given a source image x and a generated image  $\hat{x}$ , we define the identity loss as:

$$\mathcal{L}_{id} = e^{-D_{id}(F_x, F_{\hat{x}})}, \tag{14}$$

where  $F_x$  denotes the FaceNet embedding of image x and  $D_{\rm id}$  is the Euclidean L2 distance. This exponential form encourages increasing dissimilarity between the source and deidentified image in the embedding space.

Attribute Preservation Loss. To retain non-identity facial semantics, we adopt an attribute preservation loss using FaceXFormer (Narayan et al. 2024). FaceXFormer offers multiple facial analysis tasks, including attribute estimation, which measures 40 attributes originated from the CelebA dataset (Liu et al. 2015). We extract the raw attribute probability vectors from both the original and generated images and minimize their KL divergence:

$$\mathcal{L}_{\text{attr}} = D_{\text{KL}}(A_x | | A_{\hat{x}}) = \sum_{a=1}^{N_{\text{att}}} A_x^{(a)} \log \left( \frac{A_x^{(a)}}{A_{\hat{x}}^{(a)}} \right), \quad (15)$$

where  $A_x$  and  $A_{\hat{x}}$  are the attribute probability distributions predicted by FaceXFormer, and  $N_{\text{att}} = 40$ .

**Face Mask Loss.** To localize identity transformation and reduce artifacts, we apply a masked L1 loss using a facial region mask M extracted via FaceXFormer's face parser function. This helps restrict significant changes to face-related

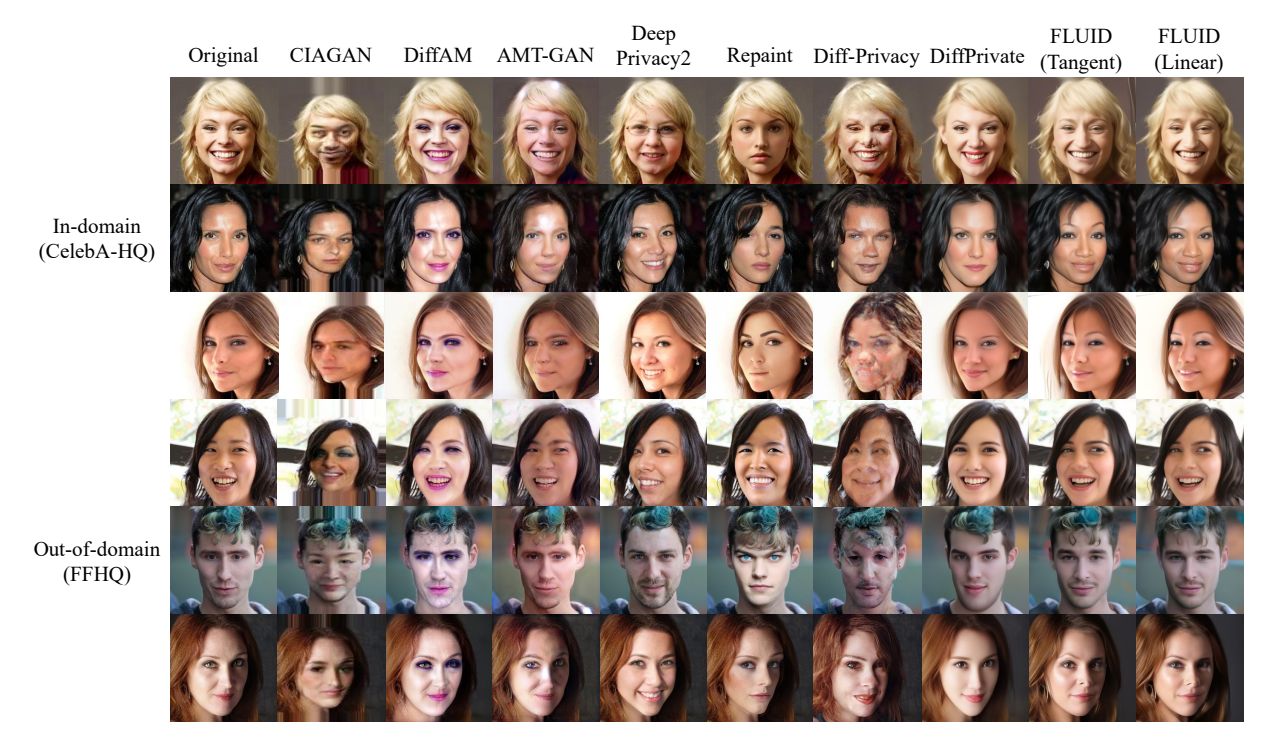


Figure 3: Qualitative comparison with SOTA face de-identification methods on in-domain (CelebA-HQ) and out-of-domain (FFHQ) images. FLUID produces de-identified face images with stricter attribute preservation than other methods. While CelebA-HQ aligns with the pretrained DM's distribution, FFHQ highlights FLUID's generalization ability to more diverse real-world inputs.

	[	CelebA-HQ					FFHQ							
Method	SID↑	Detect↑	Emotion↑	Gender↑	Pose↑	Gaze↑	Overall↑	SID↑	Detect↑	Emotion↑	Gender↑	Pose↑	Gaze↑	Overall↑
CIAGAN	0.852	0.984	0.470	0.635	0.518	0.167	0.588	0.857	0.986	0.425	0.650	0.466	0.126	0.528
DiffAM	0.507	0.999	0.500	0.810	0.774	0.514	0.653	0.515	1.000	0.493	0.763	0.767	0.473	0.648
AMT-GAN	0.492	0.999	0.653	0.855	0.787	0.658	0.681	0.408	1.000	0.668	0.841	0.821	0.638	0.623
DeepPrivacy2	0.696	1.000	0.536	0.897	0.458	0.530	0.714	0.652	1.000	0.519	0.802	0.366	0.479	0.662
Repaint	0.691	0.999	0.501	0.871	0.605	0.575	0.734	0.772	0.998	0.382	0.721	0.440	0.369	0.660
Diff-Privacy	0.921	0.982	0.543	0.686	0.586	0.407	0.756	0.901	0.987	0.504	0.711	0.536	0.320	0.711
Diffprivate	0.810	1.000	0.565	0.752	0.436	0.618	0.752	0.806	1.000	0.536	0.579	0.440	0.537	0.719
FLUID (tangent)	0.685	1.000	0.660	0.907	0.674	0.651	0.776	0.683	1.000	0.599	0.827	0.584	0.537	0.736
FLUID (linear)	0.739	1.000	0.620	0.883	0.646	0.638	$\overline{0.786}$	0.697	1.000	0.581	0.799	0.562	0.512	0.730

Table 1: Quantitative performance comparison between FLUID and SOTA face de-identification methods across six key metrics. These include identity removal (SID), image quality (detect), and preservation of four facial attributes: emotion, gender, pose, and gaze. FLUID achieves improved balance between attribute preservation and de-identification, further enhancing realism beyond other SOTA methods.

pixels, and can be written as:

$$\mathcal{L}_{\text{mask}} = \sum_{i} |x_i - \hat{x}_i| (1 - M_i), \tag{16}$$

where  $x_i$  and  $\hat{x}_i$  are the pixel values at index i in the original and generated images, respectively, and  $M_i$  is the probability face mask.

**Total Objective.** These reagent losses are combined as:

$$\mathcal{L}_{\text{total}} = \lambda_{id} \mathcal{L}_{\text{id}} + \lambda_{attr} \mathcal{L}_{\text{attr}} + \lambda_{mask} \mathcal{L}_{\text{mask}}, \quad (17)$$

where  $\lambda_{id} = 1.0$ ,  $\lambda_{attr} = 1.0$ , and  $\lambda_{mask} = 0.5$  are weights that control the relative importance of each loss term. This weighted formulation enables fine-grained control over the

trade-off between semantic fidelity and de-identification strength, offering a principled and flexible strategy for identity editing in a training-free diffusion framework.

#### **Experiments**

#### **Baselines**

To benchmark the effectiveness of our training-free facial identity editing approach, we compare it against SOTA facial de-identification models. Since no existing work addresses identity substitution in the h-space, we select representative baselines from two major categories: perturbation-based and semantic identity-shifting methods. Note that, unlike FLUID, several baselines rely on additional inputs such

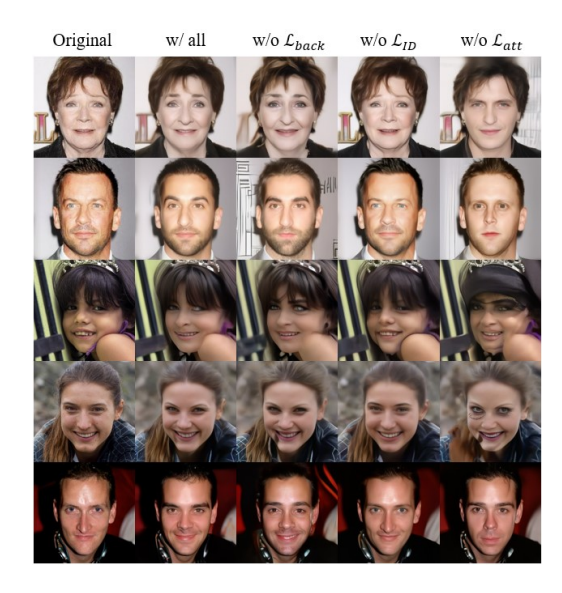


Figure 4: Qualitative results of ablation study for loss function combinations. The top two rows display CelebA-HQ samples, while the bottom three show results on FFHQ.

Method	SID↑	Detect↑	Emotion↑	Gender↑	Pose↑	Gaze↑
w/ all	0.739	1.000	0.620	0.883	0.646	0.638
w/o $\mathcal{L}_{ID}$	0.134	1.000	0.793	0.957	0.868	0.817
w/o $\mathcal{L}_{att}$	0.827	0.999	0.549	0.793	0.590	0.616
w/o $\mathcal{L}_{mask}$	0.820	0.999	0.653	0.902	0.555	0.591

Table 2: Quantitative results of ablation study based on CelebA-HQ edit results. Each loss function is omitted to assess the impact.

as reference faces, mask images, or extra training.

**Perturbation-based methods.** We include high-fidelity perturbation models that apply visual transformations without semantic reconfiguration. Specifically, we evaluate against AMT-GAN (Hu et al. 2022) and DiffAM (Sun et al. 2024). These models, often based on makeup or region masking, are favored over traditional noise- and patch-based techniques for their superior visual realism.

Semantic identity-shifting methods. We consider CIA-GAN (Maximov, Elezi, and Leal-Taixé 2020), DeepPrivacy2 (Hukkelås and Lindseth 2023), Repaint (Lugmayr et al. 2022), the edit variant of Diffprivate (Le and Carlsson 2025), and Diff-Privacy (He et al. 2024), which directly synthesize alternative identities via generative priors. We use the official implementations and default hyperparameter settings provided in their respective publications for comparison. Our method uses a fixed learning rate of lr=0.001, an editing strength parameter of  $\lambda=1000$ , and a diffusion inversion timestep of T=600.

#### **Datasets**

To evaluate our training-free identity editing framework, we adopt two standard benchmarks: CelebA-HQ (Karras

2017) and FFHQ (Karras, Laine, and Aila 2019). CelebA-HQ offers 30,000 high-resolution celebrity faces with 40 annotated binary attributes, enabling fine-grained assessment of attribute preservation. FFHQ comprises 70,000 diverse, high-quality face images, supporting evaluation under natural variations in age, pose, lighting, and ethnicity. Together, these datasets ensure a comprehensive evaluation across both structured attribute supervision and unconstrained real-world diversity.

#### **Evaluation Metrics**

To rigorously assess identity suppression, attribute preservation, and detectability, we adopt the following metrics.

**Identity Deviation.** We define identity deviation as source identity distance (SID), which indicates the difference between the original and edited images in terms of identity. We use ArcFace (Deng et al. 2019), a SOTA angular margin-based FR model, to quantify SID. This is measured as the inverse cosine similarity between ArcFace embeddings of the original image x and the de-identified result  $\hat{x}$ :

$$R_{\rm id} = 1 - \cos(F_{Arc}(x), F_{Arc}(\hat{x})),$$
 (18)

where  $F_{Arc}(\cdot)$  denotes the ArcFace encoder.

**Attribute Preservation.** To evaluate semantic consistency, we focus on gender, emotion, pose, and gaze. Gender and emotion are predicted using DeepFace (Serengil and Ozpinar 2021), and their preservation metric for each attribute  $a \in \text{gender}$ , emotion is:

$$R_a = \mathbb{I}\left[\mathsf{DeepFace}_a(x) = \mathsf{DeepFace}_a(\hat{x})\right], \quad (19)$$

where  $\mathbb{I}[\cdot]$  is the indicator function.

To evaluate pose consistency, we use the pose estimator function from FaceXFormer and compute a deviation-based preservation score that combines pitch, yaw, and roll angular differences into a single metric. Given pose deviations  $\Delta_{\text{pitch}},~\Delta_{\text{yaw}},~\text{and}~\Delta_{\text{roll}}$  between original and de-identified images, we first calculate the root mean square (RMS):

$$RMS_{pose} = \sqrt{\frac{\Delta_{pitch}^2 + \Delta_{yaw}^2 + \Delta_{roll}^2}{3}}.$$
 (20)

The pose preservation score is then normalized as:

$$R_{\text{pose}} = \max\left(0, 1 - \frac{\text{RMS}_{\text{pose}}}{\tau}\right),$$
 (21)

where  $\tau=5$  represents the angle threshold in degrees for significant pose deviation. Higher scores indicate better pose preservation, with perfect preservation yielding  $R_{\rm pose}=1$ . Inspired by Disguise (Cai et al. 2024), we include gaze as an additional utility using L2CS-Net (Abdelrahman et al. 2023), estimating pitch and yaw. The gaze preservation score reuses Equations 20 and 21, with  $\tau=15$ .

**Detectability.** To assess visual plausibility and face detectability, we count the number of face detection successes  $R_{\rm det}$ . We use both Dlib (King 2009) and MTCNN (Zhang et al. 2016) and average the counts.

**Overall Metric.** We use a *nested harmonic mean* to prevent an aggregate from over-valuing a configuration that inflates one attribute while degrading another. First, we form a harmonic mean score of four attributes:

$$HM_{attr} = \frac{4}{\frac{1}{R_{emotion}} + \frac{1}{R_{gender}} + \frac{1}{R_{pose}} + \frac{1}{R_{gaze}}},$$
 (22)

then apply another harmonic mean with three elements,  $R_{\rm id}$ ,  $R_{\rm det}$ , and  ${\rm HM_{attr}}$  to obtain the overall score  ${\rm HM_{overall}}$ . Because harmonic mean is dominated by low components, a method cannot mask weak privacy or a degraded attribute with a single strong metric; nesting enforces internal balance among attributes before combining the three pillars (privacy, detectability, semantics) concisely.

#### **Results**

**Quantitative and qualitative comparison.** Table 1 and Figure 3 present **FLUID's quantitative and qualitative performance** against existing methods. Notably, despite requiring no task-specific training and minimal attribute supervision, FLUID achieves the **best overall balance** between identity suppression and attribute preservation.

On CelebA-HQ, tangent edit yields the highest gender preservation (0.907), alongside strong emotion (0.660) and gaze (0.651) consistency, resulting in a high balance score of 0.776. While linear edits show higher SID (0.739), they introduce off-manifold artifacts, which reduce visual realism and semantic stability. In contrast, tangent-space editing, by respecting the local geometry of the *h*-space, enhances generalization to out-of-distribution data, as evidenced in FFHQ where it achieves the highest overall score (0.736). This underscores the strength of our training-free framework, matching or exceeding domain-specific methods without retraining.

**Identity disentanglement validation.** We assess whether identity-specific directions can be discovered without explicit supervision. Our optimization finds latent directions  $\Delta h_{\rm id}$  that successfully increase identity distance while maintaining stable non-identity attributes. Figure 5 illustrates this validation: as editing strength  $\lambda$  increases, identity distance (measured by MagFace (Meng et al. 2021)) grows monotonically, while attribute differences (measured by SwinFace (Qin et al. 2023)) remain consistent. This empirical evidence supports our core assumption that identity and semantics can be decoupled through loss-guided optimization.

**Tangent vs. linear editing.** Why does tangent editing outperform linear editing, and does it generalize? In high-dimensional latent spaces, linear edits often drift off the data manifold, resulting in degraded outputs. Tangent editing, conversely, constrains the edit direction to the local tangent plane of h, preserving norm and curvature (as shown in Equations 12 and 13). This geodesic formulation avoids semantic drift, significantly improving attribute preservation, visual quality, and cross-domain generalization, particularly in challenging settings like emotion and pose changes (Table 1).

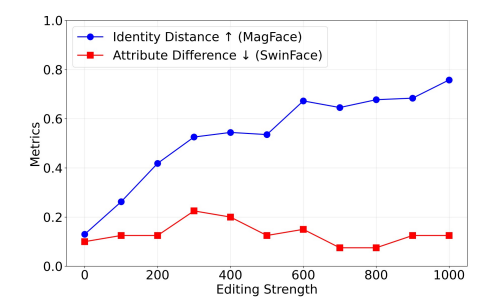


Figure 5: Identity-attribute trade-off curve across increasing linear edit strengths.

# **Ablation Study**

To evaluate the individual contribution of the proposed reagent loss components, we conduct an ablation study, summarized in Table 2 and Figure 4. Removing  $\mathcal{L}_{ID}$  severely compromises identity suppression, underscoring its critical role in effective de-identification. Excluding  $\mathcal{L}_{att}$  leads to significant semantic drift, particularly altering key attributes such as gender and facial expression, thereby violating attribute preservation. When  $\mathcal{L}_{mask}$  is omitted, we observe increased background artifacts and reduced visual realism, despite slight improvements in some numerical scores, highlighting a trade-off between perceived quality and structural integrity.

# **Limitations and Societal Impact**

While our method excels in identity suppression, attribute preservation, and visual quality, it has some limitations. Its iterative latent-space optimization hinders real-time use in resource-limited settings. Performance may drop on highly out-of-distribution data, given its design assumptions and reliance on CelebA-HQ-style priors. Also it may not reliably preserve high-frequency details (e.g., text, glasses, occlusions). First, as a training-free method relying on latent-space optimization, it requires iterative backpropagation, which may hinder real-time deployment in resourceconstrained environments. Second, although our approach generalizes across domains, its effectiveness may decline on highly out-of-distribution data, given its design assumptions and reliance on CelebA-HQ-style priors. Third, the model may not consistently preserve high-frequency details (e.g., text, glasses, occlusions), which are not explicitly optimized in our loss formulation.

#### Conclusion

We introduced FLUID, a novel training-free framework for face de-identification via identity substitution in the latent *h*-space of pretrained DMs. By leveraging disentangled reagent losses, FLUID enables fine-grained identity removal while preserving facial semantics and visual fidelity. We proposed and empirically supported both linear and geodesic (tangent-based) editing strategies, grounded by theoretical justification. Extensive experiments on CelebA-HQ and FFHQ demonstrate that FLUID achieves competi-

tive de-identification performance with outperforming balance across identity suppression, attribute preservation, and image quality, all without requiring additional training or auxiliary data. This work opens promising directions for controllable, explainable, and privacy-preserving face editing, with practical implications for secure data sharing, ethical AI applications, and real-world de-identification systems.

#### References

- Abdal, R.; Zhu, P.; Mitra, N. J.; and Wonka, P. 2021. Styleflow: Attribute-conditioned exploration of stylegangenerated images using conditional continuous normalizing flows. *ACM Transactions on Graphics (ToG)*, 40(3): 1–21.
- Abdelrahman, A. A.; Hempel, T.; Khalifa, A.; Al-Hamadi, A.; and Dinges, L. 2023. L2cs-net: Fine-grained gaze estimation in unconstrained environments. In 2023 8th International Conference on Frontiers of Signal Processing (ICFSP), 98–102. IEEE.
- Ashenhurst, J. 2012a. Comparing the SN1 and SN2 Reactions. Accessed: 2025-06-25.
- Ashenhurst, J. 2012b. The SN1 Mechanism. https://www.masterorganicchemistry.com/2012/07/13/the-sn1-mechanism/. Accessed: 2025-08-02.
- Avrahami, O.; Lischinski, D.; and Fried, O. 2022. Blended diffusion for text-driven editing of natural images. In *Proceedings of the IEEE/CVF conference on computer vision and pattern recognition*, 18208–18218.
- Babaguchi, N.; Koshimizu, T.; Umata, I.; and Toriyama, T. 2009. Psychological study for designing privacy protected video surveillance system: PriSurv. *Protecting Privacy in Video Surveillance*, 147–164.
- Cai, Z.; Gao, Z.; Planche, B.; Zheng, M.; Chen, T.; Asif, M. S.; and Wu, Z. 2024. Disguise without disruption: Utility-preserving face de-identification. In *Proceedings of the AAAI Conference on Artificial Intelligence*, volume 38, 918–926.
- Chen, T.; Xu, B.; Zhang, C.; and Guestrin, C. 2016. Training deep nets with sublinear memory cost. *arXiv preprint arXiv:1604.06174*.
- Choi, J.; Lee, J.; Shin, C.; Kim, S.; Kim, H.; and Yoon, S. 2022. Perception prioritized training of diffusion models. In *Proceedings of the IEEE/CVF conference on computer vision and pattern recognition*, 11472–11481.
- Deng, J.; Guo, J.; Xue, N.; and Zafeiriou, S. 2019. Arcface: Additive angular margin loss for deep face recognition. In *Proceedings of the IEEE/CVF conference on computer vision and pattern recognition*, 4690–4699.
- Dhariwal, P.; and Nichol, A. 2021. Diffusion models beat gans on image synthesis. *Advances in neural information processing systems*, 34: 8780–8794.
- European Union. 2016. Regulation (EU) 2016/679 (General Data Protection Regulation). Official Journal of the European Union, L119, 1–88.
- Goodfellow, I. J.; Pouget-Abadie, J.; Mirza, M.; Xu, B.; Warde-Farley, D.; Ozair, S.; Courville, A.; and Bengio, Y.

- 2014. Generative adversarial nets. Advances in neural information processing systems, 27.
- Government of India. 2023. Digital Personal Data Protection Act, 2023. Ministry of Law and Justice.
- Haas, R.; Huberman-Spiegelglas, I.; Mulayoff, R.; Graßhof, S.; Brandt, S. S.; and Michaeli, T. 2024. Discovering interpretable directions in the semantic latent space of diffusion models. In 2024 IEEE 18th International Conference on Automatic Face and Gesture Recognition (FG), 1–9. IEEE.
- Hahm, J.; Lee, J.; Kim, S.; and Lee, J. 2024. Isometric representation learning for disentangled latent space of diffusion models. *arXiv preprint arXiv:2407.11451*.
- Härkönen, E.; Hertzmann, A.; Lehtinen, J.; and Paris, S. 2020. Ganspace: Discovering interpretable gan controls. *Advances in neural information processing systems*, 33: 9841–9850.
- He, X.; Zhu, M.; Chen, D.; Wang, N.; and Gao, X. 2024. Diff-privacy: Diffusion-based face privacy protection. *IEEE Transactions on Circuits and Systems for Video Technology*.
- Ho, J.; Jain, A.; and Abbeel, P. 2020. Denoising diffusion probabilistic models. *Advances in neural information processing systems*, 33: 6840–6851.
- Hu, S.; Liu, X.; Zhang, Y.; Li, M.; Zhang, L. Y.; Jin, H.; and Wu, L. 2022. Protecting facial privacy: Generating adversarial identity masks via style-robust makeup transfer. In *Proceedings of the IEEE/CVF conference on computer vision and pattern recognition*, 15014–15023.
- Hukkelås, H.; and Lindseth, F. 2023. Deepprivacy2: Towards realistic full-body anonymization. In *Proceedings of the IEEE/CVF winter conference on applications of computer vision*, 1329–1338.
- Ilia, P.; Polakis, I.; Athanasopoulos, E.; Maggi, F.; and Ioannidis, S. 2015. Face/off: Preventing privacy leakage from photos in social networks. In *Proceedings of the 22nd ACM SIGSAC Conference on computer and communications security*, 781–792.
- Jeong, J.; Kwon, M.; and Uh, Y. 2024. Training-free content injection using h-space in diffusion models. In *Proceedings of the IEEE/CVF Winter Conference on Applications of Computer Vision*, 5151–5161.
- Karras, T. 2017. Progressive Growing of GANs for Improved Quality, Stability, and Variation. *arXiv preprint arXiv:1710.10196*.
- Karras, T.; Laine, S.; and Aila, T. 2019. A style-based generator architecture for generative adversarial networks. In *Proceedings of the IEEE/CVF conference on computer vision and pattern recognition*, 4401–4410.
- Kim, G.; Kwon, T.; and Ye, J. C. 2022. Diffusionclip: Text-guided diffusion models for robust image manipulation. In *Proceedings of the IEEE/CVF conference on computer vision and pattern recognition*, 2426–2435.
- Kim, M.; Liu, F.; Jain, A.; and Liu, X. 2023. Dcface: Synthetic face generation with dual condition diffusion model. In *Proceedings of the ieee/cvf conference on computer vision and pattern recognition*, 12715–12725.

- King, D. E. 2009. Dlib-ml: A machine learning toolkit. *The Journal of Machine Learning Research*, 10: 1755–1758.
- Kwon, M.; Jeong, J.; and Uh, Y. 2022. Diffusion models already have a semantic latent space. *arXiv preprint arXiv:2210.10960*.
- Le, M.-H.; and Carlsson, N. 2025. DiffPrivate: Facial Privacy Protection with Diffusion Models. *Proceedings on Privacy Enhancing Technologies*.
- Liu, Z.; Luo, P.; Wang, X.; and Tang, X. 2015. Deep learning face attributes in the wild. In *Proceedings of the IEEE international conference on computer vision*, 3730–3738.
- Lugmayr, A.; Danelljan, M.; Romero, A.; Yu, F.; Timofte, R.; and Van Gool, L. 2022. Repaint: Inpainting using denoising diffusion probabilistic models. In *Proceedings of the IEEE/CVF conference on computer vision and pattern recognition*, 11461–11471.
- Maximov, M.; Elezi, I.; and Leal-Taixé, L. 2020. Ciagan: Conditional identity anonymization generative adversarial networks. In *Proceedings of the IEEE/CVF conference on computer vision and pattern recognition*, 5447–5456.
- Meng, Q.; Zhao, S.; Huang, Z.; and Zhou, F. 2021. Magface: A universal representation for face recognition and quality assessment. In *Proceedings of the IEEE/CVF conference on computer vision and pattern recognition*, 14225–14234.
- Muñoz, C.; Zannone, S.; Mohammed, U.; and Koshiyama, A. 2023. Uncovering bias in face generation models. *arXiv* preprint arXiv:2302.11562.
- Narayan, K.; VS, V.; Chellappa, R.; and Patel, V. M. 2024. Facexformer: A unified transformer for facial analysis. *arXiv* preprint arXiv:2403.12960.
- Prabhu, V. U.; Yap, D. A.; Wang, A.; and Whaley, J. 2019. Covering up bias in CelebA-like datasets with Markov blankets: A post-hoc cure for attribute prior avoidance. *arXiv* preprint arXiv:1907.12917.
- Qin, L.; Wang, M.; Deng, C.; Wang, K.; Chen, X.; Hu, J.; and Deng, W. 2023. SwinFace: A multi-task transformer for face recognition, expression recognition, age estimation and attribute estimation. *IEEE Transactions on Circuits and Systems for Video Technology*, 34(4): 2223–2234.
- Rizzo, R. 2005. Chapter 11: Substitution Reactions SN1 and SN2 Mechanisms. https://www.vanderbilt.edu/AnS/Chemistry/Rizzo/chem220a/Ch11slides.pdf. Accessed: 2025-06-25.
- Ronneberger, O.; Fischer, P.; and Brox, T. 2015. U-net: Convolutional networks for biomedical image segmentation. In *Medical image computing and computer-assisted intervention–MICCAI 2015: 18th international conference, Munich, Germany, October 5-9, 2015, proceedings, part III 18, 234–241.* Springer.
- Schroff, F.; Kalenichenko, D.; and Philbin, J. 2015. Facenet: A unified embedding for face recognition and clustering. In *Proceedings of the IEEE conference on computer vision and pattern recognition*, 815–823.
- Serengil, S. I.; and Ozpinar, A. 2021. Hyperextended light-face: A facial attribute analysis framework. In 2021 International Conference on Engineering and Emerging Technologies (ICEET), 1–4. IEEE.

- Shaheryar, M.; Lee, J. T.; and Jung, S. K. 2024. IDDiffuse: Dual-Conditional Diffusion Model for Enhanced Facial Image Anonymization. In *Proceedings of the Asian Conference on Computer Vision*, 4017–4033.
- Shaheryar, M.; Lee, J. T.; and Jung, S. K. 2025. Black Hole-Driven Identity Absorbing in Diffusion Models. In *Proceedings of the Computer Vision and Pattern Recognition Conference*, 28544–28554.
- Shan, S.; Wenger, E.; Zhang, J.; Li, H.; Zheng, H.; and Zhao, B. Y. 2020. Fawkes: Protecting privacy against unauthorized deep learning models. In *29th USENIX security symposium* (*USENIX Security 20*), 1589–1604.
- Shen, Y.; Yang, C.; Tang, X.; and Zhou, B. 2020. Interfacegan: Interpreting the disentangled face representation learned by gans. *IEEE transactions on pattern analysis and machine intelligence*, 44(4): 2004–2018.
- Song, J.; Meng, C.; and Ermon, S. 2020. Denoising diffusion implicit models. *arXiv preprint arXiv:2010.02502*.
- Stypułkowski, M.; Vougioukas, K.; He, S.; Zięba, M.; Petridis, S.; and Pantic, M. 2024. Diffused heads: Diffusion models beat gans on talking-face generation. In *Proceedings of the IEEE/CVF Winter Conference on Applications of Computer Vision*, 5091–5100.
- Sun, Y.; Yu, L.; Xie, H.; Li, J.; and Zhang, Y. 2024. Diffam: Diffusion-based adversarial makeup transfer for facial privacy protection. In *Proceedings of the IEEE/CVF conference on computer vision and pattern recognition*, 24584–24594.
- Terhorst, P.; Kolf, J. N.; Damer, N.; Kirchbuchner, F.; and Kuijper, A. 2020. SER-FIQ: Unsupervised estimation of face image quality based on stochastic embedding robustness. In *Proceedings of the IEEE/CVF conference on computer vision and pattern recognition*, 5651–5660.
- Wen, Y.; Liu, B.; Ding, M.; Xie, R.; and Song, L. 2022. Identitydp: Differential private identification protection for face images. *Neurocomputing*, 501: 197–211.
- Westerlund, M. 2019. The emergence of deepfake technology: A review. *Technology innovation management review*, 9(11).
- Wu, Z.; Lischinski, D.; and Shechtman, E. 2021. Stylespace analysis: Disentangled controls for stylegan image generation. In *Proceedings of the IEEE/CVF conference on computer vision and pattern recognition*, 12863–12872.
- Zhang, K.; Zhang, Z.; Li, Z.; and Qiao, Y. 2016. Joint face detection and alignment using multitask cascaded convolutional networks. *IEEE signal processing letters*, 23(10): 1499–1503.
- Zhao, W.; Rao, Y.; Shi, W.; Liu, Z.; Zhou, J.; and Lu, J. 2023. Diffswap: High-fidelity and controllable face swapping via 3d-aware masked diffusion. In *Proceedings of the IEEE/CVF Conference on Computer Vision and Pattern Recognition*, 8568–8577.
- Zhu, Y.; Wu, Y.; Deng, Z.; Russakovsky, O.; and Yan, Y. 2023. Boundary guided learning-free semantic control with diffusion models. *Advances in Neural Information Processing Systems*, 36: 78319–78346.

# **Supplementary Material**

In this supplementary material, we provide the following:

- Detailed explanation on SN1, the substitution reaction in organic chemistry that we used as a metaphor.
- Algorithm flow of our method.
- Experiments and source of hyperparameter selection.
- User study on human identification of de-identified faces.
- Failure cases, especially produced by FFHQ results.

#### The Metaphor

In organic chemistry, a substitution reaction refers to the process of replacing one functional group in a molecule with another, while largely preserving the rest of the molecular structure (Rizzo 2005; Ashenhurst 2012a). Among such reactions, the SN1 (unimolecular nucleophilic substitution) mechanism proceeds in two distinct stages. First, the leaving group spontaneously departs, resulting in the formation of a highly reactive, electron-deficient carbocation intermediate. This unstable intermediate reflects a vulnerable yet reorganizable state. In the second step, a nucleophile selectively attacks the carbocation, completing the substitution and stabilizing the molecule.



Figure 6: The  $S_N1$  mechanism illustrated in (Ashenhurst 2012b).

In contrast, the SN2 (bimolecular nucleophilic substitution) mechanism is a single-step reaction where the nucle-ophile directly replaces the leaving group at a fixed site, without forming an intermediate. SN2 is deterministic and rigid, typically operating only when the substitution site is clearly accessible and unambiguous.

This distinction forms the conceptual foundation of our approach. We draw a parallel between molecular substitution and identity editing in diffusion models. We conceptualize the latent representation of a facial image as a molecular structure in which identity acts as a substitutable functional group, embedded within a stable semantic backbone encoding attributes such as pose, expression, lighting, and age. Just as substitution reactions allow targeted replacement of molecular components while preserving overall structure, we aim to selectively replace identity in latent space while retaining all non-identity semantics.

Our method aligns naturally with the SN1 mechanism. First, we do not assume the identity subspace is predefined. Instead, we dynamically discover and suppress identity directions in the latent space via loss-guided optimization, analogous to the formation of the carbocation intermediate. Once identity is removed, we get an anonymized identity vector, akin to a nucleophile completing the substitution.

This two-step, context-aware, and optimization-driven process mirrors the SN1 mechanism in both structure and intent. Moreover, unlike SN2, our method does not rely on a fixed, interpretable site for substitution, but instead adapts to the distributional geometry of the latent space, reinforcing the relevance of the SN1 analogy. This metaphor offers a conceptually intuitive and technically grounded framework for controlled, semantic-preserving identity substitution in the latent space of diffusion models.

#### **Procedure of FLUID**

On top of Figure 2 in main paper, we provide our method's flow using pseudocodes in Algorithm 1. Our method starts with initialization, where an identity embedding, an attribute distribution, and a face mask are obtained by auxiliary models given an input image. A direction vector  $\Delta h_{id}$  is initialized randomly as a vector with a small norm m. Then  $\Delta h_{\rm id}$ and the original image's vector z are fused by either linear (Equation 7) or tangent edit (Equations 12 and 13), producing an edited vector  $\hat{z}$ . The optimization steps proceed by repeatedly calculating losses between the input images and the edited image (Equation 17), made by decoding  $\hat{z}$  (Equation 8), while backpropagating the loss values to  $\Delta h_{\rm id}$  to correct it (Equation 11). After a given number of steps  $n_{opt}$ , the final vector  $\hat{z}$  is decoded through the DM's denoising process, yielding a de-identified image  $\hat{x}$ . For all random initializations and possible operations, our random seed is fixed with the value of 1006.

Inspired by spherical interpolation's success in other generative models, we therefore traverse edits along local tangent planes, controlling the angular step size to stay within the observed shell. As Figure 7 and Table 1 show, this angular traversal yields fewer artifacts and better quality than straight linear edits, which can wander significantly beyond the typical norm range into areas where the decoder produces unrealistic outputs.

#### **Hyperparameter Selection and Analysis**

Reagent loss weights. We conducted ablation studies on loss weights, and the results are reported in Table 4. The cases of 0 for each weight are excluded because the results are presented in Table 2.  $\lambda_{\rm id}=0.5$  and  $\lambda_{\rm id}=1.5$  each lead to the weakest and strongest SID scores, making the identity loss trivial and dominant, respectively. Lowering  $\lambda_{\text{attr}}$  results in lower attribute preservation rates but higher SID due to weaker constraints. However, both damage the balances, which are proven by low overall scores. Increasing  $\lambda_{\text{mask}}$ forces the background information to be fixed firmly and limits the editable region for de-identification. In this case, the optimization process decides to alter the gender information to compensate for the difficulty. Although  $\lambda_{\text{mask}} = 0.5$ shows a slightly lower balance score than  $\lambda_{id} = 1.5$ , we select it for superior emotion preservation at the cost of moderately lower SID. This configuration ( $\lambda_{\text{mask}} = 0.5$ ) is applied to the reported experiments in the main paper.

**Denoising steps and computational analysis.** Similarly, we conduct another ablation study to select the number of denoising steps. As written in Table 3, increasing the number

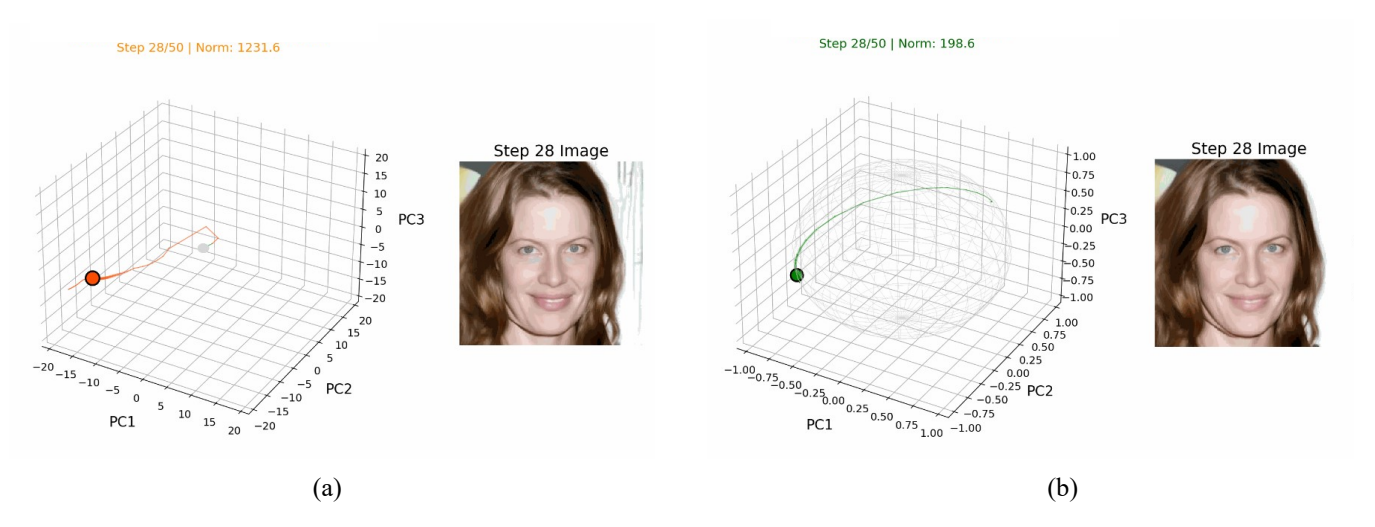


Figure 7: Comparison of linear against tangent edits in the h-space. We fit a 3-dimensional principal component analysis (PCA) pool with 5000 vectors sampled from 100 editing trajectories, and project the desired vectors onto this PCA space to visualize their trajectory. (a) Linear edits apply raw  $\Delta h_{\rm id}$ , allowing the vector norm to drift beyond the typical shell and producing visual artifacts. (b) Tangent edits project  $\Delta h_{\rm id}$  onto the local tangent plane at a constant norm, constraining the trajectory and reducing artifacts.

of reverse steps tend to reduce SID and retain attributes, especially gaze. Although 8 denoising steps show the best balance with the strongest SID, we select 16 steps for our experiments for improved stability and consistency, ensuring reliable performance across diverse inputs and more attribute preservation. Even though the number of denoising steps is much less than that of DDPM, thanks to the implementation of deterministic denoising by DDIM (Song, Meng, and Ermon 2020), naively backpropagating through the iterative reverse steps still requires considerable amount of memory. Therefore, we implement gradient checkpointing (Chen et al. 2016) to significantly reduce memory consumption, enabling us to run the implementation on our hardware, a single Titan XP GPU with 12GB of memory. With the help of gradient checkpointing, FLUID runs with approximately 6GB of memory and takes under 3 seconds for each optimization step, including all auxiliary model operations.

For the duration of injecting the edited h vector  $\hat{z}$ , we mostly follow Asyrp as:

$$p_{\theta}^{(t)}(x_{t-1} \mid x_t) = \mathcal{N}\left(\sqrt{\alpha_{t-1}} \mathbf{P}_t \left(\epsilon_{\theta}^t(x_t)\right) + \mathbf{D}_t, \sigma_t^2 \mathbf{I}\right). \tag{23}$$

The form of  $\epsilon_{\theta}^{t}(\cdot)$ , the usage of guidance  $\Delta h_{id}$ , and the randomness factor  $\eta$  depend on timestep t:

- If T ≥ t ≥ t<sub>edit</sub>, the model uses η = 0 and guided prediction: 
   <sup>ℓ</sup><sub>θ</sub>(x<sub>t</sub> | Δh<sub>id</sub>).
- If  $t_{\text{edit}} > t \ge t_{\text{boost}}$ , the model uses  $\eta = 0$  and unconditional prediction:  $\epsilon_{\theta}^{t}(x_{t})$ .
- If  $t_{\rm boost} > t$ , the model also uses unconditional prediction:  $\epsilon_{\theta}^t(x_t)$  but  $\eta = 1$ .

Our choice of starting timestep T=600 and editing range  $t_{\rm edit}=400$  is motivated by converging evidence from recent work on DM semantics and the critical 'mixing step' concept. P2 weighting (Choi et al. 2022) demonstrates that

DMs learn perceptually rich semantic content at medium signal-to-noise ratio (SNR) timesteps, while Boundary Diffusion (Zhu et al. 2023) provides theoretical and empirical evidence for a 'mixing step' around t = 500 where semantic boundaries emerge in the latent space. Through Markov chain mixing time analysis, the authors use t = 500 in their implementation as the critical convergence point where unconditional DMs begin to exhibit meaningful semantic structure. By restricting our  $\Delta h_{\rm id}$  injection to timesteps [600, 400], we strategically target this semantically rich region that spans the critical mixing step at  $t \approx 500$ , ensuring that identity-specific transformations occur precisely where semantic boundaries are most well-defined. This approach leverages both the content-learning stage identified by P2 weighting and the semantic boundary formation demonstrated by Boundary Diffusion, enabling more effective identity suppression while maintaining semantic consistency of non-identity facial attributes and avoiding interference with coarse structural learning at higher timesteps.

On the other hand, our choice of  $t_{\rm boost}=200$  follows the implementation of Asyrp, which timesteps lower than that enable  $\eta=1$  to avoid additional noise over the resulting image and improve details. Therefore, our denoising strategy consists of edited information injection  $(600 \ge t > 400)$ , unconditional denoising  $(400 \ge t > 200)$ , and quality boosting  $(200 \ge t > 0)$ .

**Linear edit strength.** In the main paper, we clarify that the editing strength  $\lambda$  for linear edits is set to 1000. In contrast, Boundary Diffusion offers the editing strength within the range of [-150,150], as its direction vector encodes the signed distance to a hyperplane (i.e., boundary) defined by a linear SVM. Since we do not rely on such boundaries during optimization, and the norm of  $\Delta h_{\rm id}$  varies throughout the process, we conduct an ablation study on the linear edit-

#### **Algorithm 1:** Flow of FLUID **Input:** Input image x, pretrained decoder D, weights $\lambda_{\rm id}, \lambda_{\rm attr}, \lambda_{\rm mask}$ , step size $\eta$ , editing type (linear or tangent), initialized $\Delta h_{\rm id}$ 's norm m, number of optimization steps $n_{\text{opt}}$ . Initialize: $z \leftarrow f_{\text{inv}}(x)$ ⊳ Equation 6 $\Delta h_{\rm id} \sim \mathcal{N}(0, I) \times m$ **Optimization:** for $n \leftarrow 1$ to $n_{opt}$ do if editing type is linear then $\hat{z} \leftarrow z + \lambda \cdot \Delta h_{id}$ ⊳ Equation 7 else $z_{\text{unit}} \leftarrow z/\|z\|, \quad \Delta h_{\text{unit}} \leftarrow \Delta h_{\text{id}}/\|\Delta h_{\text{id}}\|$ $\Delta h_{\text{proj}} \leftarrow \Delta h_{\text{unit}} - \langle \Delta h_{\text{unit}}, z_{\text{unit}} \rangle \cdot z_{\text{unit}} \triangleright \text{Equation}$ 12 $\hat{z} \leftarrow ||z|| \cdot (\cos(\theta) \cdot z_{\text{unit}} + \sin(\theta) \cdot \Delta h_{\text{proj}})$ Equation 13 $\mathcal{L}_{total} = \lambda_{id} \mathcal{L}_{id} + \lambda_{attr} \mathcal{L}_{attr} + \lambda_{mask} \mathcal{L}_{mask} \triangleright Equation 17$ ⊳ Equation 11 $\Delta h_{\rm id} \leftarrow \Delta h_{\rm id} - \eta \cdot \nabla_{\Delta h_{\rm id}} \mathcal{L}_{\rm total}$ **return** De-identified image $\hat{x}$

Method	SID↑	Detect↑	Emotion↑	Gender↑	Pose↑	Gaze↑	Overall↑
8 steps	0.858	0.999	0.579	0.873	0.610	0.543	0.799
12 steps	0.762	1.000	0.586	0.843	0.630	0.617	0.782
16 steps	0.739	1.000	0.620	0.883	0.646	0.638	0.786
20 steps	0.651	0.999	0.634	0.876	0.681	0.641	0.755
24 steps	0.624	1.000	0.616	0.870	0.679	0.652	0.741

Table 3: Quantitative results on the number of denoising steps used for optimization.

ing strength  $\lambda$  in the range of 100 to 1000, as shown in Table 5. Unlike other ablation studies where trade-offs are evident, we observe trivial trade-off patterns in this case. Larger values of  $\lambda$  consistently lead to increased SID, with constantly high detectability scores and slightly decreasing attribute preservation, thereby improving the overall score. We attribute the increase in SID to a larger exploration range enabled by stronger scaling factors within a limited number of optimization steps. Based on this observation, we select  $\lambda = 1000$  as our default linear edit strength.

**Optimization steps.** In Table 6, we show the impact of the number of optimization steps on the overall performance. The identity-attribute trade-off is also shown here by 10 and 20 steps with low SID and high attribute preservation, indicating insufficiency in de-identification strength and, ultimately, optimization steps. We select 50 steps for our experiments due to the high SID at the cost of a minor decrease in attribute preservation rates. While a higher number of steps yields better overall balance and more iterations might further marginally improve, our results show that 50 steps already achieve competitive performance compared to SOTA methods, validating our approach.

**Evaluation thresholds.** To evaluate pose and gaze preservation, we set the thresholds  $\tau=5$  and  $\tau=15$  for pose

Method	SID↑	Detect↑	Emotion↑	Gender↑	Pose↑	Gaze↑	Overall↑
All = 1.0	0.686	1.000	0.602	0.844	0.615	0.670	0.759
$\lambda_{\mathrm{id}} = 0.5$	0.659	1.000	0.596	0.895	0.666	0.668	0.756
$\lambda_{\mathrm{id}} = 1.5$	0.775	0.999	0.532	0.876	0.648	0.666	0.788
$\lambda_{ m attr}=0.5$	0.751	1.000	0.493	0.830	0.624	0.657	0.765
$\lambda_{ m attr}=1.5$	0.670	1.000	0.593	0.888	0.639	0.656	0.756
$\lambda_{ m mask}=0.5$	0.737	1.000	0.620	0.883	0.646	0.638	0.786
$\lambda_{\text{mask}} = 1.5$	0.679	1.000	0.541	0.880	0.646	0.675	0.754

Table 4: Quantitative results of ablation study on each loss function weight, with updated metrics and nested harmonic-mean "Overall." Other weights not mentioned for each case are set to the default value of 1.0.

λ	SID↑	Detect†	Emotion↑	Gender†	Pose↑	Gaze↑	Overall↑
100	0.569	1.000	0.653	0.915	0.696	0.665	0.723
200	0.641	1.000	0.659	0.902	0.677	0.654	0.756
300	0.674	1.000	0.643	0.904	0.671	0.655	0.768
400	0.692	0.999	0.630	0.893	0.668	0.646	0.772
500	0.695	1.000	0.663	0.899	0.665	0.632	0.776
600	0.710	1.000	0.651	0.880	0.646	0.636	0.778
700	0.716	1.000	0.620	0.872	0.627	0.635	0.773
800	0.721	1.000	0.634	0.870	0.624	0.630	0.776
900	0.722	1.000	0.620	0.877	0.640	0.637	0.778
1000	0.739	1.000	0.620	0.883	0.646	0.638	0.786

Table 5: Quantitative results of ablation study on each linear edit strength  $\lambda$  used for linear edits.

and gaze, respectively. These values represent the maximum allowable deviations, beyond which pose and gaze angle differences are regarded as significantly distorted. The thresholds are determined based on the distribution of raw angular deviations, as presented in Tables 7 and 8. In Table 7, Repaint from FFHQ exhibits the largest distortion in pose pitch angle, motivating the choice of  $\tau=5$  for pose. Similarly, Table 8 shows that CIAGAN yields the greatest gaze pitch deviation on the FFHQ dataset, justifying the selection of  $\tau=15$  for gaze.

# **Evaluating Human Recognition on De-identified Faces**

We conducted a user study to show how human perception detects de-identified faces. We design a simple graphical user interface (GUI) built on Python that shows an image once at a time and asks users to guess whether the image has been de-identified by a generative model or not. We first select 15 de-identified images each from all compared methods and FLUID, and 20 real images from CelebA-HQ, with all images chosen from those with high SER-FIQ (Terhorst et al. 2020) scores. This is to prevent the users from identifying fake images from mere artifacts generated by models, which could easily guide the users to identify the fakeness without looking at the faces. We ask 25 graduate students with diverse nationalities who are not familiar with the field of face de-identification. Note that we do not disclose the number of images selected from each category to the users, nor do we reveal any additional information about the face image that appears in the GUI. An example screenshot of our GUI is shown in Figure 8, while the results and example

$n_{step}$	SID↑	Detect↑	Emotion↑	Gender↑	Pose↑	Gaze↑	Overall↑
10	0.431	0.999	0.687	0.924	0.742	0.705	0.646
20	0.568	0.999	0.674	0.921	0.692	0.666	0.724
30	0.649	1.000	0.638	0.900	0.676	0.647	0.755
40	0.708	1.000	0.612	0.890	0.657	0.630	0.773
50	0.739	1.000	0.620	0.883	0.646	0.638	0.786
60	0.771	0.999	0.622	0.892	0.624	0.603	0.791

Table 6: Quantitative results of ablation study on the number of optimization steps.

	(	CelebA-HÇ	)	FFHQ			
Method	Pitch↓	Yaw↓	Roll↓	Pitch↓	Yaw↓	Roll↓	
Ours (linear)	2.63	1.57	0.84	3.22	1.94	1.01	
Ours (tangent)	2.39	1.58	0.80	3.07	1.91	0.99	
Diffprivate	3.24	3.52	0.99	3.49	3.24	0.92	
Repaint	2.89	1.55	0.97	4.25	2.00	1.22	
Diff-Privacy	2.77	1.85	1.33	3.16	1.93	1.57	
DeepPrivacy2	3.26	2.71	2.01	3.94	3.09	2.26	
CIAGAN	3.44	1.95	1.35	3.69	2.40	1.41	
AMT-GAN	1.51	0.87	0.61	1.15	0.83	0.62	
DiffAM	1.50	0.90	0.87	1.57	0.97	0.81	

Table 7: Raw pitch, yaw, and roll angle deviations of each method measured by the pose estimator from FaceXFormer. Pitch angle difference from Repaint under FFHQ shows the greatest deviation of 4.25.

	Celeb	A-HQ	FFI	HQ
Method	Pitch↓	Yaw↓	Pitch↓	Yaw↓
Ours (linear)	5.96	4.83	8.45	5.98
Ours (tangent)	5.71	4.72	8.07	5.59
Diffprivate	6.51	4.81	8.00	5.69
Repaint	8.21	6.22	10.66	8.08
Diff-Privacy	10.32	7.16	11.95	8.07
DeepPrivacy2	8.15	5.73	8.66	6.87
CÎAGAN	14.45	10.18	14.62	9.98
AMT-GAN	5.24	5.03	5.55	5.33
DiffAM	9.12	4.79	9.68	5.58

Table 8: Raw pitch and yaw angle deviations of each method measured by L2CS-Net. Pitch angle difference from CIA-GAN under FFHQ shows the greatest distortion of 14.62.

images are illustrated in Figure 9 and 10, respectively.

Besides FLUID achieving the lowest human recognition rate (0.31), counterintuitively, DeepPrivacy2 has attained a low human recognition rate as well (0.33) despite its low overall score in Table 1. We attribute this to the following responses collected after the blind test, in which the participants were asked to explain the primary factors that led them to conclude an image was de-identified.

Quality degradation by various artifacts. Noise-like artifacts from CIAGAN and Diff-Privacy make it obvious to recognize the presense of de-identification. DiffAM's makeups also belong to this category, offering better results than noise- or patch-based methods, but still suboptimal to be realistic. Users were also able to detect subtle boundaries marked by abrupt color changes across the line, which are commonly observed in mask-based inpainting models such

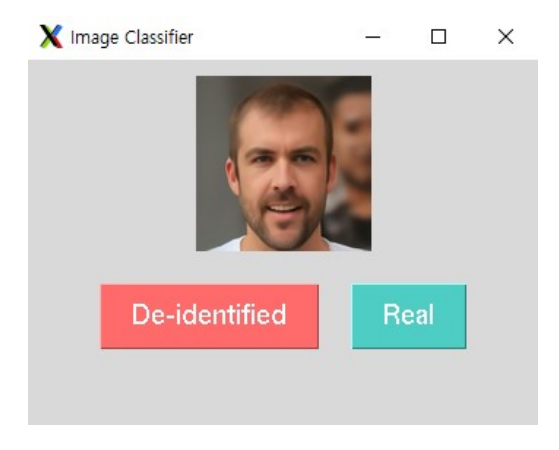


Figure 8: The GUI interface for our user study. Users are asked to decide whether the given images are processed by a de-identification method or not. The image name and source are hidden for fair blind test.

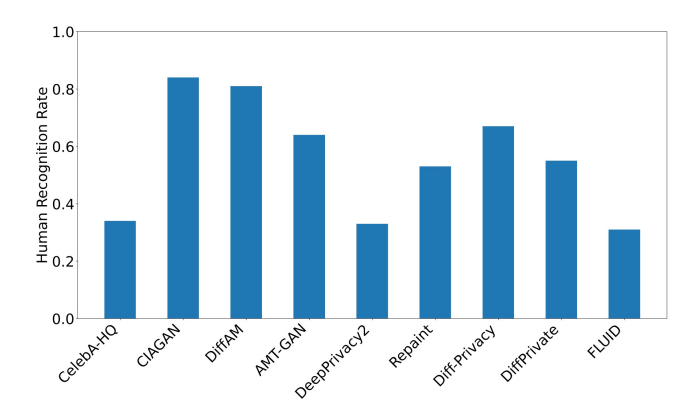


Figure 9: Human recognition of de-identification results based on our user study. FLUID and DeepPrivacy2 are considered the most realistic, showing similar recognition rates to that of CelebA-HQ.

as Repaint. Although we intentionally selected the bestquality results throughout all methods, the typical generation performances of these models remain in the selection.

Mismatching gender information. Often the de-id entification was recognized by unusual mixtures of gender-related attributes. For example, the fusion of common attributes seen from women's images and those from men's (e.g., a bald woman) tend to be identified as fake. Similarly, some users would classify fake images by observing facial skeletal morphologies. In this case, FLUID and DeepPrivacy2 were able to avoid such decisions by showing high gender preservation rates, minimizing the odds of distorting gender information.

**Too-perfect images.** DiffPrivate's results were likely to be recognized as de-identified due to perfect-clean skin and hairlines, which are unlikely to be seen in real-world scenarios. FLUID and DeepPrivacy2's results were less recognized as synthesized due to natural skin tones and hair ap-

"Unusual combination of gender-related attributes."

"Too perfect to be real."

Not recognized as fake

Figure 10: Example images corresponding to each frequently observed user response in our study. Participants frequently recognized low-quality outputs from perturbation-based methods and identified borderline artifacts introduced by inpainting techniques. Additionally, unusual mixtures of gender representations raised user suspicion regarding the authenticity of the data. Notably, the overly perfect appearance of some faces, such as unnaturally clear skin textures and overly smooth hairlines, was also cited as an indicator that the images had been generated or modified by AI models.

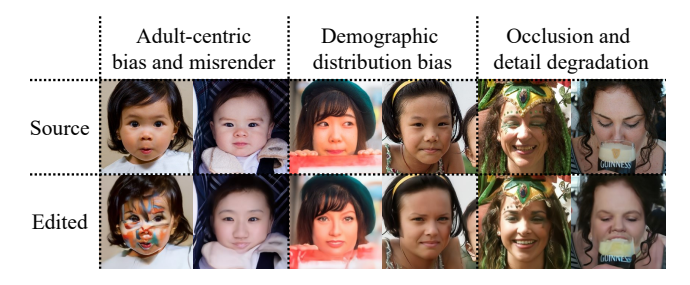


Figure 11: Failure examples and biases from out-of-domain FFHQ edit results.

pearances.

#### Customizable de-identification.

In many real-world applications, complete attribute preservation during de-identification may not be desirable or necessary. For instance, medical researchers studying facial expressions in autism spectrum disorders may need to preserve emotional attributes while removing identity-related features. Conversely, demographic studies might require preserving gender attributes while obscuring other characteristics. This necessitates a flexible approach where practitioners can selectively choose which attributes to modify during the de-identification process.

In organic chemistry, and especially in combinatorial chemistry, extensive combinations of reagents are used to examine many different types of reaction results. This adds up to our metaphor because such chemical experiments typically do not require time-intensive training-like processes

to test the reagent combinations. Similarly, we modify the behavior of the attribute reagent loss by partially fixing components of the source attribute distribution. While our method originally targeted the full distribution of the source image—thereby preserving overall attributes—we now assign varying probability values to specific attributes, ranging from 0.1 to 0.9, to explore targeted manipulations along with de-identification. Results of changing {'Male', 'Narrow Eyes' and {'Smile', 'Mouth Slightly Open'} are shown in Figure 12. When attributes 'Smile' and 'Mouth Slightly Open' are assigned low probabilities, the de-identified faces appear neutral. A high probability for 'Mouth Slightly Open' and a low one for 'Smile' produce an emotionless face with an open mouth. Conversely, assigning a high probability to 'Smile' and a low one to 'Mouth Slightly Open' generates a closed-mouth smile. High probabilities for both yield a grin. Adjusting the probabilities of 'Male' and 'Narrow Eyes' also produces interpolated effects. This supports our claim that customizable de-identification can be realized training-free, just like conducting combinatorial chemistry experiments.

#### **Failure Examples and Dataset Bias**

Figure 11 shows representative failure cases in which our method produces noticeable quality degradation and artifacts on challenging inputs. These failures occur primarily for images that lie outside the CelebA-HQ training distribution of the DM. First, the adult-centric generation tendency renders infant faces with adult-like features or severe distortions. Second, the demographic distribution bias occasionally shifts facial characteristics and geometry toward stereotypical White ethnicity, effectively 'whitening' the minority faces. Finally, faces with heavy occlusions and fine details, such as glasses or jewelry, are frequently simplified or frontalized, losing important structural cues. These limitations reflect both the celebrity-centric biases of the training data and the inherent smoothing effects of diffusion representations (Prabhu et al. 2019; Muñoz et al. 2023). Although our method delivers competitive performance, these failure modes stress the challenges when extending to more diverse, real-world inputs.

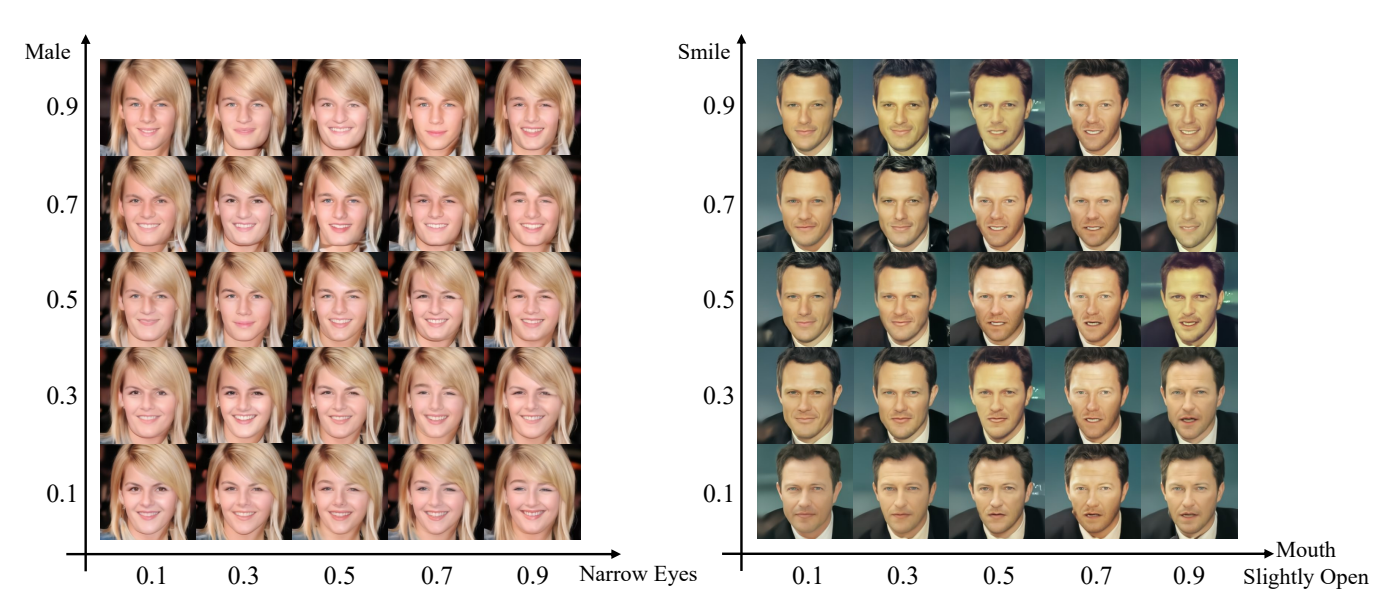


Figure 12: Additional examples demonstrating customizable de-identification. Images are de-identified with the attribute values in the source attribute distribution for 'Smile' and 'Mouth Slightly Open', and 'Male' and 'Narrow eyes' fixed from 0.1 to 0.9.